

# DCE-FORMER: A TRANSFORMER-BASED MODEL WITH MUTUAL INFORMATION AND FREQUENCY-BASED LOSS FUNCTIONS FOR EARLY AND LATE RESPONSE PREDICTION IN PROSTATE DCE-MRI

Sadhana S<sup>1</sup> Sriprabha Ramanarayanan<sup>1,2</sup> Arunima Sarkar<sup>1</sup>  
 Matcha Naga Gayathri<sup>1</sup> Keerthi Ram<sup>2</sup> Mohanasankar Sivaprakasam<sup>1,2</sup>

<sup>1</sup> Indian Institute of Technology Madras (IITM), India

<sup>2</sup> Healthcare Technology Innovation Centre (HTIC), IITM, India

## ABSTRACT

Dynamic Contrast Enhanced Magnetic Resonance Imaging aids in the detection and assessment of tumor aggressiveness by using a Gadolinium-based contrast agent (GBCA). However, GBCA is known to have potential toxic effects. This risk can be avoided if we obtain DCE-MRI images without using GBCA. We propose, DCE-former, a transformer-based neural network to generate early and late response prostate DCE-MRI images from non-contrast multimodal inputs (T2 weighted, Apparent Diffusion Coefficient, and T1 pre-contrast MRI). Additionally, we introduce (i) a mutual information loss function to capture the complementary information about contrast uptake, and (ii) a frequency-based loss function in the pixel and Fourier space to learn local and global hyper-intensity patterns in DCE-MRI. Extensive experiments show that DCE-former outperforms other methods with improvement margins of +1.39 dB and +1.19 db in PSNR, +0.068 and +0.055 in SSIM, and -0.012 and -0.013 in Mean Absolute Error for early and late response DCE-MRI, respectively.

**Index Terms**— DCE-MRI, transformer, Mutual Information, frequency loss, contrast-enhancing patterns

## 1. INTRODUCTION

The Dynamic Contrast Enhanced Magnetic Resonance Imaging (DCE-MRI) sequence produces a visualization of angiogenesis and highlights subtle tumor lesions. The increased permeability of tumor vessels is imaged with a contrast agent such as Gadolinium (Gad) which washes in and out of the tumor more rapidly than normal tissue. DCE-MRI involves early-phase and late-phase contrast enhanced imaging to capture the morphological characteristics of the tumor over time. However, there are safety concerns around Gad retention and its potential toxic effects [1]. It is beneficial to reduce the dosage or avoid the Gad contrast agent. The existing DCE-MRI involves anatomic acquisitions such as T1 pre-contrast and T2-Weighted (T2W) MRI, along with Apparent Diffusion

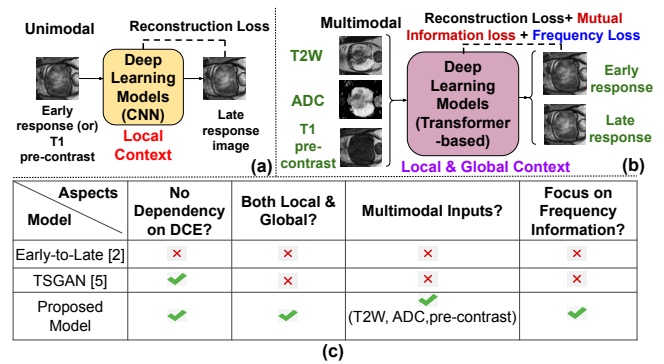


**Fig. 1.** Concept diagram of DCE-MRI synthesis approaches (a) Previous methods focus on local contextual learning from early response using CNNs and without ADC information. (b) & (c) The proposed DCE-Former is a transformer-based network that learns both local and global pixel dependencies, captures semantic details and contrast-enhancing patterns using mutual information and frequency-based loss functions.

Coefficient (ADC), which quantifies water molecule diffusion within the tissue. The purpose of this work is to synthesize early and late-phase DCE-MRI given such non-contrast images which capture structural and perfusion information.

Synthetic MRI, enabled by deep learning, has been explored for reducing or eliminating Gad-based imaging in brain cancer [2]. Deep Generative Adversarial Networks (GAN) is a prominent method with prior works exploring low-dose and cross-modality MRI synthesis [3]. In [4], a deep learning model is proposed for generating full-dose late response images from both pre-contrast and low-dose images for brain MRI. A conditional GAN with a tailor-made contrast enhancement loss function [5] is formulated to generate late response from early response in Breast MRI images. TSGAN [6] focuses on synthesizing DCE-MRI images from non-contrast MRI images. Inspired by the multimodal learning capabilities to capture salient, mutual, and complementary information from multiple modalities, the encoder-decoder

convolutional neural network (CNN) [7] [2] and Hi-Net [8] synthesize brain MR images by fusing the latent representations of multimodal MR images.

Unlike prior works (Fig.1), we consider the problem of synthesizing both early and late response images of DCE-MRI from multimodal non-contrast inputs by using a transformer-based model to capture local and global contrast details as the dynamics of the contrast in DCE acquisitions might not be localized to a particular region within the prostate. In particular, we use Uformer [9] which offers core benefits making it extensible to image synthesis tasks, namely (i) the Locally Enhanced Window (LeWin) transformer blocks, and (ii) multi-scale restoration modulator to capture local and global dependencies to generate details from all feature locations at hierarchical levels synergistically. Furthermore, to effectively combine the physiological features that involve time-varying contrast-enhancing patterns of normal and diseased tissue types, we use two loss components (i) mutual information-based loss to capture nonlinear statistical dependencies between multimodal inputs and predicted images, distinct from the approach in [10], and (ii) frequency-based loss function in both the spatial and Fourier domains [11] to preserve the contrast levels of the DCE-MRI images and finer details like local hyper-enhancement of intensities within lesions. We summarize our contributions as,

1. We propose DCE-former, a transformer-based architecture, in a GAN network to synthesize early and late-phase prostate DCE-MRI images from multimodal inputs such as T2W, ADC, and T1 pre-contrast images.
2. We propose two loss functions, (i) a mutual information-based loss function to capture the complementary information about contrast uptake in DCE-MRI, and (ii) a frequency-based loss function in the pixel and Fourier space to learn local and global hyper-intensity patterns.
3. Extensive experiments, using ProstateX dataset, show that the proposed DCE-former predicts the early and late response DCE-MR images with improvement margins of (i) +1.39 dB PSNR, +0.068 SSIM, -0.012 MAE, -18.00 FID for early response, and (ii) +1.19 dB PSNR, +0.055 SSIM, -0.013 MAE, -15.29 FID for late response, over the second best-performing baseline model, ResViT.

## 2. METHODOLOGY

### 2.1. Early and Late response using GANs

The image synthesizing task can be formulated using GANs by coercing the generated post-contrast early and late response images to be as plausible as the ground truth post-contrast DCE images while learning the spatial coherence, tissue dynamics, and perfusion information from the input  $\tilde{X}$ .  $\tilde{X}$  is concatenation of T2W, ADC and T1 pre-contrast images ( $\tilde{X} = X_{T2,ADC,pre}$ ). This adversarial approach is given by,

$$G(\tilde{X})^* = \arg \min_G \max_D \left( G(\tilde{X}), D(Y_{e,l}) \right) L_{GAN}. \quad (1)$$

### 2.2. Mutual Information (MI) Loss

The reconstruction loss component ( $\mathcal{L}_1$ ), which computes pixel-wise differences, might not capture the perceptually relevant characteristics of the image, like textural details in the time-varying contrast patterns [12]. To drive the model to generate temporal contrast enhancement patterns coherently, we use the MI loss function to learn representations that yield high semantic similarity with regard to the underlying tissue information between the real and generated images. The MI loss,  $\mathcal{L}_{MI}$ , between the real early (and late) response images and the generated early (and late) response is given by,

$$MI(X_i; G(\tilde{X})) = H(X_i) + H(G(\tilde{X})) - H(X_i, G(\tilde{X}))$$

$$\mathcal{L}_{MI}(G) = \frac{2 * MI(X_i; G(\tilde{X}))}{H(X_i) + H(G(\tilde{X}))} \quad (2)$$

Here,  $X_i$  and  $G(\tilde{X})$  are the real and fake DCE-MR images, where  $i$  denotes the early (or late) response image.  $H(X_i)$  and  $H(G(\tilde{X}))$  denote the individual entropy of the images and  $H(X_i, G(\tilde{X}))$  denotes the joint entropy. Our main objective is to maximize the mutual information between the ground truth and generated early and late response images.

### 2.3. Frequency Loss

The frequency loss function [11] aids in learning local and global features at the optimization level as (i) Convolution by Gaussian kernel in spatial domain represents frequency features in a local manner (ii) Discrete Fourier Transform (DFT) characterizes frequency distribution globally as each spatial frequency is computed by employing information from all pixels. The high-frequency (HF) component,  $X_H$ , of the image, which preserves fine-grained contrast details, is computed from the low (LF) component,  $X_L$ , which is obtained by applying a Gaussian kernel, as follows.

$$X_H = X - X_L \quad (3)$$

The spatial domain reconstruction loss term for both low-frequency and high-frequency components is given by,

$$\mathcal{L}_{rec,pix}(G) = E[\|X_L - (G(X))_L\|_1 + \|X_H - (G(X))_H\|_1] \quad (4)$$

For the frequency domain loss function, we apply the DFT ( $F$ ) on the image. The frequency spectrum reconstruction loss is regulated as,

$$\mathcal{L}_{rec,fft}(G) = E[\|F^R(X) - F^R(G(X))\|_1] \quad (5)$$

The overall loss is formulated as,

$$G^* = \arg \min_G \max_D (G, D) L_{GAN} + \lambda_1 \mathcal{L}_1 + (1 - \lambda_{MI}) \mathcal{L}_{MI}(G) + \lambda_{rec,pix} \mathcal{L}_{rec,pix}(G) + \lambda_{rec,fft} \mathcal{L}_{rec,fft}(G)$$

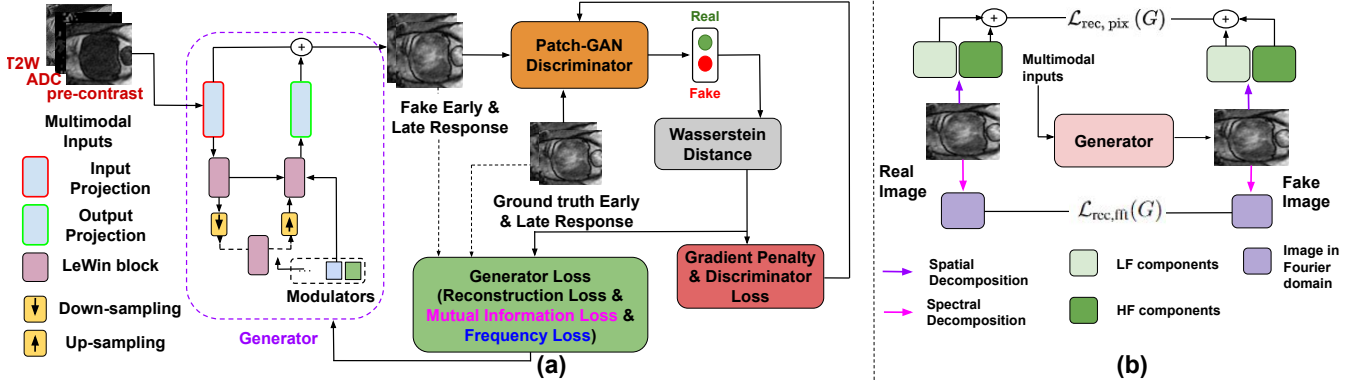


**Fig. 2.** (a) DCE-former architecture consists of Uformer as the generator and PatchGAN discriminator with the two loss components (MI-based and frequency-based) to optimize the model weights. (b) The proposed frequency loss function computes the loss in the low and high-frequency components in the spatial and spectral domains.

**Table 1.** Quantitative Comparison of the synthesized early & late DCE-MRI timepoints between DCE-former & other models

Model	Early Response				Late Response			
	PSNR $\uparrow$	SSIM $\uparrow$	MAE $\downarrow$	FID Score $\downarrow$	PSNR $\uparrow$	SSIM $\uparrow$	MAE $\downarrow$	FID Score $\downarrow$
ConvLSTM	14.92 +/- 1.50	0.2397 +/- 0.04	0.1393	118.706	15.27 +/- 2.56	0.2392 +/- 0.06	0.1351	115.480
Pix2Pix	15.21 +/- 5.49	0.2886 +/- 0.18	0.1121	65.8695	13.80 +/- 5.05	0.2321 +/- 0.19	0.1288	32.8592
ResViT	21.46 +/- 0.04	0.6369 +/- 0.04	0.0638	32.4624	20.88 +/- 0.04	0.6231 +/- 0.05	0.0684	30.0611
RegGAN	20.56 +/- 0.02	0.5966 +/- 0.02	0.0571	23.7963	20.09 +/- 0.02	0.5803 +/- 0.02	0.0617	22.6124
TSGAN	21.16 +/- 3.50	0.6253 +/- 0.10	0.0693	23.7533	20.46 +/- 2.64	0.5926 +/- 0.09	0.0749	24.6665
<b>DCE-former</b>	<b>22.85 +/- 3.74</b>	<b>0.7047 +/- 0.11</b>	<b>0.0522</b>	<b>14.4614</b>	<b>22.07 +/- 3.33</b>	<b>0.6790 +/- 0.13</b>	<b>0.0558</b>	<b>14.7617</b>

where  $\lambda_1$ ,  $\lambda_{MI}$ ,  $\lambda_{rec, pix}$  and  $\lambda_{rec, fft}$  are the weight hyperparameters for each component of the loss function.

### 3. DATASET & IMPLEMENTATION DETAILS

We have used ProstateX dataset [13] which consists of the 346 patients' studies acquired without an endo-rectal coil consisting of 5520 images, (4416 and 1104 images for training and validation respectively). Each patient data consists of T2W, ADC, T1 pre-contrast and DCE-MRI images. We used SimpleITK rigid registration framework to align all the images. The prostate organ is cropped to a size of  $160 \times 160 \times 16$ .

The proposed DCE-former (in Fig.2) is a Wasserstein GAN with Gradient Penalty (WGAN-GP) with Uformer [9] as the generator and a Patch-GAN discriminator. We have compared DCE-former with five models, namely Pix2Pix [14], ConvLSTM [15], ResViT [16], RegGAN [17] and TSGAN [6]. We fixed the middle time point as the early response image and the last time point as the late response image in the ground truth DCE-MRI sequences with varying numbers of time points across studies. In the transformer network, we have fixed the number of LeWin blocks as  $\{1, 2, 8, 8\}$  in the corresponding levels of the encoder and the decoder. The optimal Gaussian kernel size (for the frequency loss) is  $13 \times 13$  for our curated dataset. All models are implemented in

Pytorch 2.0 and are trained for 200 epochs, batch size = 6, and hyperparameters,  $\lambda_1 = 5$ ,  $\lambda_{MI} = 10$ ,  $\lambda_{rec, pix} = 10$  and  $\lambda_{rec, fft} = 10$ . The evaluation metrics are PSNR, SSIM, MAE (Mean Absolute Error), and FID (Frechet Inception Distance).

### 4. RESULTS

Our experiments include (i) a comparative study against other GAN methods for contrast translation, (ii) an ablative study of the various loss components used in our approach and (iii) an analysis of the contribution of ADC images in synthesizing DCE-MR images. Table 1 shows the quantitative comparison of the proposed approach with other methods. Our observations are: (i) Our model (for both early and late response images) outperforms all the other methods consistently across all the evaluation metrics. (ii) Our model also performs better than the standard MRI image-to-image translation benchmark, ResViT. Visual comparison in Fig.3(a) shows that our DCE-former is able to generate the hyperintensity patterns in the early and late response images very close to the ground truth as compared to other methods. We believe that the reason for this observation is that our approach learns essential details from ADC images which have the potential to reflect the perfusion properties of tissues. Furthermore, the structural correlation between the multimodal inputs and the out-

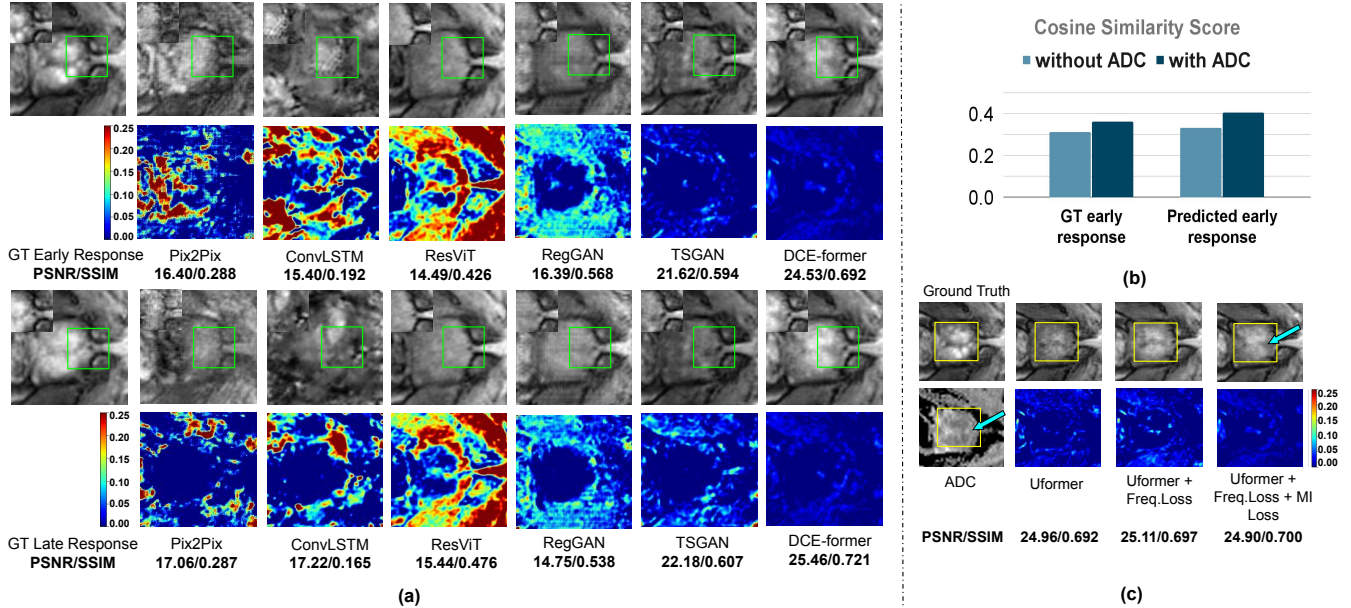


**Fig. 3.** (a) Visual results of early & late response (from left to right): Ground truth, Pix2Pix, ConvLSTM, ResViT, RegGAN, TSGAN, and DCE-former (ours) (b) Comparison of similarity scores between predicted & ground truth early response images with & without ADC in multimodal input. (c) Qualitative results for the ablative study. A combination of both MI and frequency loss effectively captures the contrast enhancement patterns. The DCE-MRI predictions image shows matching and complementary features with respect to the ADC (as shown by blue arrows). Green and yellow boxes denote the regions of interest.

puts is learned using T2W and T1 pre-contrast MRI images. (iii) Although TSGAN generates images with comparatively less residual error, it is unable to capture the exact contrast behavior due to its limited capability of long-range dependencies. Our DCE-former overcomes this limitation by leveraging global and local contextual learning at both architecture and optimization levels. (iv) MI helps to capture the matching and complementary features from the multimodal inputs during optimization in synthesizing DCE-MRI images. Aided by frequency loss, the fine-grained contrast details are learned in both spatial and frequency domains. From Figure 3(c), we see that the matching complementary features refer to dark and bright (hyperintense) regions in the ADC and DCE-MRI images, respectively. Wilcoxon signed-rank test shows that our metrics are statistically significant ( $p < 0.05$ ).

#### 4.1. Ablative Studies

**Ablative Study with ADC:** Figure 3(b) emphasizes the importance of learning from ADC images during training. We note that the similarity for real (and synthesized) DCE-MRI images is higher when ADC is used as input compared to the case with inputs without ADC. This is due to the strong correlation between DCE-MRI and ADC images.

**Ablative Study of the loss components:** In this study, we understand the contributions of optimizing the network using each of the three loss functions. From Table 2, we note that the L1 loss which minimizes pixel-wise differences is inad-

**Table 2.** Ablative study on the loss components

Model	DCE-MRI output	
	PSNR	SSIM
$\mathcal{L}_1$	23.01 +/- 3.72	0.6880 +/- 0.113
$\mathcal{L}_1 + \mathcal{L}_{rec,pix} + \mathcal{L}_{rec,fft}$	23.08 +/- 3.73	0.6919 +/- 0.113
$\mathcal{L}_1 + \mathcal{L}_{rec,pix} + \mathcal{L}_{rec,fft} + \mathcal{L}_{MI}$	23.03 +/- 3.44	0.7047 +/- 0.119

equate in capturing physiological details. Both MI and DFT loss components play a key role in improving the overall perceptual quality of the prediction and a suitable combination of both components improves the quality further. The visual results in Figure 3(c) affirm these observations qualitatively.

## 5. CONCLUSION

We propose DCE-former, transformer-based model in a GAN setting to synthesize early and late response images in DCE-MRI from multimodal inputs such as T2W, ADC, and T1 pre-contrast images. To generate post-contrast patterns, we establish an MI loss and frequency-based loss which leverage the global and local contextual learning of the transformer to capture the physiological features and complementary information about contrast intake. We are currently extending our approach to predict pharmacokinetic parametric maps to estimate various physiological parameters in DCE-MRI.

## 6. COMPLIANCE WITH ETHICAL STANDARDS

This research study was conducted retrospectively using human subject data made available in open access by the Cancer Imaging Archive. Ethical approval was not required as confirmed by the license attached with the open-access data.

## 7. ACKNOWLEDGMENTS

Acknowledgement withheld.

## 8. REFERENCES

- [1] Moshe Rogosnitzky and Stacy Branch, “Gadolinium-based contrast agent toxicity: a review of known and proposed mechanisms,” *Biometals*, vol. 29, no. 3, pp. 365–376, 2016.
- [2] Chao Chen, Catalina Raymond, William Speier, Xinyu Jin, Timothy F. Cloughesy, Dieter Enzmann, Benjamin M. Ellingson, and Corey W. Arnold, “Synthesizing mr image contrast enhancement using 3d high-resolution convnets,” *IEEE Transactions on Biomedical Engineering*, vol. 70, no. 2, pp. 401–412, 2023.
- [3] Biting Yu, Yan Wang, Lei Wang, Dinggang Shen, and Luping Zhou, “Medical image synthesis via deep learning,” *Deep Learning in Medical Image Analysis: Challenges and Applications*, pp. 23–44, 2020.
- [4] Enhao Gong, M. John, Max Wintermark Pauly, and Greg Zaharchuk, “Deep learning enables reduced gadolinium dose for contrast-enhanced brain mri,” in *Journal of magnetic resonance imaging*, 2018, vol. 48, pp. 330–340.
- [5] J. C. Caicedo R. D. Fonnegra, M. Liliana Hernandez and G. M. Díaz, “Early-to-late prediction of dce-mri contrast-enhanced images in using generative adversarial networks,” in *2023 IEEE 20th International Symposium on Biomedical Imaging*, 2023, pp. 1–5.
- [6] E. Kim, H. H. Cho, J. Kwon, Y. T. Oh, E. S. Ko, and H. Park, “Tumor-attentive segmentation-guided gan for synthesizing breast contrast-enhanced mri without contrast agents,” in *IEEE journal of translational engineering in health and medicine*, 2022, pp. 32–43.
- [7] A. Chartsias, M. V. Giuffrida T. Joyce, and S. A. Tsafaris, “Multimodal mr synthesis via modality-invariant latent representation,” in *IEEE Transactions on Medical Imaging*, 2018, vol. 37, pp. 803–814.
- [8] T. Zhou, G. Chen H. Fu, and L. Shao J. Shen, “Hinet: Hybrid-fusion network for multi-modal mr image synthesis,” in *IEEE Transactions on Medical Imaging*, 2020, vol. 39, pp. 2772–2781.
- [9] Zhendong Wang, Xiaodong Cun, Jianmin Bao, Wengang Zhou, Jianzhuang Liu, and Houqiang Li, “Uformer: A general u-shaped transformer for image restoration,” in *Proceedings of the IEEE/CVF Conference on Computer Vision and Pattern Recognition (CVPR)*, 2022, pp. 17683–17693.
- [10] M.I. Belghazi, A. Baratin, S. Rajeswar, S. Ozair, Y. Bengio, R.D. Hjelm, and A.C. Courville, “Mutual information neural estimation,” in *International Conference on Machine Learning*, 2018.
- [11] M. Cai, H. Zhang, H. Huang, Q. Geng, and G. Huang, “Frequency domain image translation: More photo-realistic, better identity-preserving,” in *Proceedings of the IEEE/CVF International Conference on Computer Vision*, 2021, pp. 13910–13920.
- [12] C. Ledig, L. Theis, F. Huszár, J. Caballero, A. Cunningham, A. Acosta, and W. Shi, “Photo-realistic single image super-resolution using a generative adversarial network,” in *Proceedings of the IEEE conference on computer vision and pattern recognition*, 2017, pp. 4681–4690.
- [13] Oscar Debats Geert Litjens, Nico Karssemeijer Jelle Barentsz, and Henkjan Huisman, “Prostatectomy challenge data,” in *The Cancer Imaging Archive*, 2017.
- [14] Phillip Isola, Jun-Yan Zhu, Tinghui Zhou, and Alexei A Efron, “Image-to-image translation with conditional adversarial networks,” in *Proceedings of the IEEE Conference on Computer Vision and Pattern Recognition (CVPR)*, 2017, pp. 5967–5976.
- [15] Xingjian GulrajSHI, Zhourong Chen, Hao Wang, Dit-Yan Yeung, Wai-kin Wong, and Wang-chun WOO, “Convolutional lstm network: A machine learning approach for precipitation nowcasting,” in *Advances in Neural Information Processing Systems*, 2015, vol. 28.
- [16] O. Dalmaz, M. Yurt, and T. Çukur, “Resvit: Residual vision transformers for multimodal medical image synthesis,” in *IEEE Transactions on Medical Imaging*, 2022, vol. 41, pp. 2598–2614.
- [17] L. Kong, C. Lian, D. Huang, Y. Hu, and Q. Zhou, “Breaking the dilemma of medical image-to-image translation,” in *Advances in Neural Information Processing Systems*, 2021, vol. 34, pp. 1964–1978.